Colloids and Surfaces A: Physicochemical and Engineering Aspects 685 (2024) 133234

Contents lists available at ScienceDirect

Colloids and Surfaces A: Physicochemical and Engineering Aspects

journal homepage: www.elsevier.com/locate/colsurfa

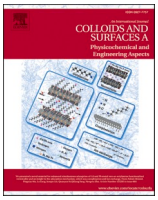

Investigation of silica particle growth by incorporation of a pyrene fluorescent probe

Fabian Walther, Dominik Brühwiler *

ZHAW Zurich University of Applied Sciences, Institute of Chemistry and Biotechnology, CH-8820 Wädenswil, Switzerland

GRAPHICAL ABSTRACT

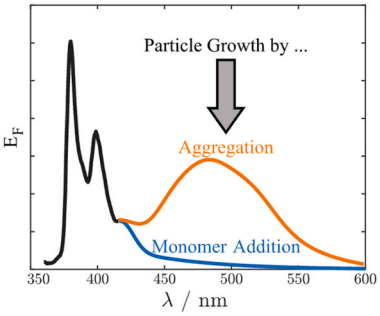

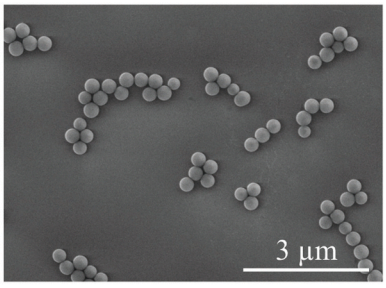

ARTICLE INFO

Keywords:
Stöber
Silica
Particle
Fluorescence
Excimer
Pyrene
Growth
Aggregation
Monomer addition

ABSTRACT

The growth of silica particles synthesized by the Stöber method was investigated by the co-condensation of pyrene sulfonyl chloride (PySCl) coupled to (3-aminopropyl)triethoxysilane (APTES). Growth by monomer addition could be distinguished from growth by aggregation based on the intensity of the pyrene excimer emission of the resulting particles. The influence of the base concentration, water/ethanol ratio, solvent, temperature, and type of silica precursor was studied. At high hydrolysis rates, the growth occurred primarily by aggregation, whereas growth by monomer addition was predominant at low hydrolysis rates. The results were confirmed by evaluating the accessibility of the co-condensed pyrene moieties and by determining the porosity of the particles.

1. Introduction

In 1968, Stöber, Fink and Bohn [1] reported a robust process for the production of monodisperse silica particles, which later became known as the Stöber process. The scope of application of silica particles is broad and includes diverse fields such as chromatography [2], ceramics [3], catalysis [4], drug delivery [5], and forensics [6]. Despite of the fact that the Stöber method has frequently been used and adapted for the synthesis of silica particles, reports on the growth mechanism tend to be controversial [7]. Two general growth mechanisms have been suggested for silica particles, namely growth by monomer addition [8–10] and by aggregation [11,12]. Growth by monomer addition typically produces

* Corresponding author.
E-mail address: dominik.bruehwiler@zhaw.ch (D. Brühwiler).

https://doi.org/10.1016/j.colsurfa.2024.133234
Received 17 October 2023; Received in revised form 10 January 2024; Accepted 11 January 2024
Available online 14 January 2024

non-porous particles [10], whereas growth by aggregation results in microporous particles [11–13]. However, inconsistencies have been reported regarding the porosity of Stöber-type silica particles. A comparison of independent studies on the production of Stöber-type silica particles reveals that pore volumes measured by nitrogen adsorption at 77 K vary over a wide range (0.001 to 0.633 $cm^3 \cdot g^{-1}$) [14–27], although similar reaction conditions were applied. Understanding the growth mechanism and the effect of the various reaction parameters on the properties of the product particles is essential for developing robust and reproducible syntheses.

Growth mechanisms have been studied by transmission electron microscopy [28,29], NMR [10,28,29], Raman scattering [8,30], dynamic light scattering [8,9], and small-angle X-ray scattering [31]. In this work, the growth mechanism is investigated by the co-condensation of pyrene sulfonyl chloride (PySCl) coupled to (3-aminopropyl)triethoxysilane (APTES). Pyrene has previously been employed to study spatial distributions in various structures by means of its excimer fluorescence [32–34]. As the distance between two pyrene units becomes smaller than 0.5 nm, excimer fluorescence occurs, which can be clearly distinguished from the fluorescence of spatially separated pyrene units [35–39]. The co-condensation of PySCl-APTES conjugates with tetraethoxysilane (TEOS) by monomer addition is expected to lead to a homogeneous distribution of the functional moieties throughout the resulting silica framework [40]. Given a low PySCl-APTES/TEOS molar ratio, the probability of creating closely spaced pyrene moieties that would lead to excimer emission is therefore small. Growth by aggregation, on the other hand, is likely to generate situations where surface-anchored pyrene moieties are located in close vicinity. Interparticle excimer formation has indeed been observed when studying the interactions of pyrene-labeled silica particles [41]. The high ratio between the external surface area and the volume of the primary particles contributes to the increased probability of excimer formation during growth by aggregation. We thus start from the hypothesis that the two general growth mechanisms lead to different fluorescence spectra of the co-condensed particles, in particular regarding the pyrene excimer band, which is expected to be absent in the case of growth by monomer addition and present in the case of growth by aggregation. Moreover, the relative vibronic band intensities of the pyrene monomer fluorescence are polarity dependent [42]. Consequently, the accessibility of the co-condensed pyrene units can be evaluated by using solvents of different polarity and thus provides independent evidence of porosity, which was additionally measured by nitrogen sorption.

2. Material & methods

2.1. Materials

2-Propanol (99.9 %), 1-butanol (99 %), acetone (99 %), aqueous ammonia (28–30 %), chlorosulfonic acid (99 %), cyclohexane (99 %), dichloromethane (99.8 %), dimethylsulfoxide (99 %), methanol (99.9 %), phosphorus pentachloride (for synthesis), pyrene (98 %), tetraethoxysilane (TEOS, 99.0 %), tetramethoxysilane (TMOS, 99 %), (3-aminopropyl)triethoxysilane (APTES, 99 %), and (3-aminopropyl)trimethoxysilane (APTMS, 97 %) were purchased from Sigma-Aldrich. Ethanol (98 %) was purchased from Reuss. Ethanol absolute (99.9 %) was obtained from VWR Chemicals. All chemicals were used as received.

2.2. Synthesis of pyrene sulfonyl chloride (PySCl)

The synthesis of PySCl was conducted according to literature (sulfonation [43], chlorination [44]). For the preparation of the pyrene sulfonate, pyrene (1200 mg, 5.93 mmol) was dissolved in dichloromethane (8 mL). The solution was cooled to 0 °C with an ice/water bath within 20 min. Subsequently, chlorosulfonic acid (793 mg, 6.3 mmol) was added dropwise within 15 min. The reaction mixture was stirred for 3 h at 0 °C and monitored by thin layer chromatography. As soon as no more pyrene was present, 1 M NaOH (15 mL, 15 mmol) was added over a period of 5 min. The reaction mixture turned from black to yellow and stirring was continued until no black particles were visible (ca. 20 min). The suspension was filtered off and the crude product was dried at room temperature for 3 d. This stage was mostly quantitative. For the second stage, the pyrene sulfonate obtained in the first stage (1800 mg, 5.92 mmol) was placed in dichloromethane (95 mL) and PCl_5 (3967 mg, 19.0 mmol) was added. The reaction mixture was heated to 40 °C and left at this temperature for 1 h. The resulting mixture was placed in a separating funnel (250 mL) and extracted with water (two times 100 mL). The organic phase was removed on a rotary evaporator under reduced pressure at a bath temperature of 45 °C. A light yellow/orange solid was obtained. The crude product was purified by normal phase column chromatography using 100 g of silica gel with dichloromethane as a mobile phase yielding 1385 mg (78 %) of a yellow/orange solid (R_F = 0.64, cyclohexane/ethyl acetate 6:4). NMR data of the product is given in the Supporting Information.

2.3. Synthesis of Stöber-type silica particles

Classical Stöber particles were synthesized according to a previously published procedure [45]. A polypropylene beaker (250 mL, diameter = 70 mm) was fitted with a magnetic stir bar (length = 47 mm). A solution of ultrapure water (43 mL), ethanol (98 %, 50 mL), and aqueous ammonia (28–30 %, 14 mL) was prepared, covered with a watch glass, and allowed to stir at 350 rpm for 10 min. After 10 min, the stirring speed was increased to 500 rpm and TEOS (8 mL) was added rapidly (< 3 s). The polypropylene beaker was covered with a watch glass and the mixture was stirred for 4 h at room temperature and 500 rpm. After 4 h, the resulting suspension was transferred to two Falcon tubes (50 mL) and centrifuged at 4000 rpm for 10 min. The particles were washed with water (three times 20 mL per Falcon tube) and ethanol (once with 20 mL). The product was oven-dried at 80 °C for 16 h.

2.4. Co-condensation of PySCl-APTES (standard procedure, sample 1)

In a headspace vial (20 mL), PySCl (18.6 mg) in ethanol (99.9 %, 5 mL) was mixed with APTES (84.51 μL) and left to stir for 16 h at 350 rpm and room temperature. TEOS (8 mL) was added to this solution and allowed to homogenize at 350 rpm for 10 min (precursor solution). In a polypropylene beaker (250 mL, diameter = 70 mm), which was equipped with a magnetic stir bar (length = 47 mm), a solution of ultrapure water (43 mL), ethanol (98 %, 45 mL) and aqueous ammonia (28–30 %, 14 mL) was prepared, covered with a watch glass, and left to stir at 350 rpm for 10 min (hydrolysis solution). After 10 min, the stirring speed of the hydrolysis solution was increased to 500 rpm and the precursor solution was added quickly (< 3 s). The polypropylene beaker was covered with a watch glass and the mixture was stirred for 4 h at room temperature and 500 rpm. After the reaction time, the resulting suspension was transferred to two Falcon tubes (50 mL) and centrifuged at 4000 rpm for 10 min. The particles were washed with water (three times 20 mL per Falcon tube) and ethanol (six times 20 mL). The product was oven-dried at 80 °C for 16 h.

2.5. Co-condensation of PySCl-APTES (proof of concept, sample 3)

In a headspace vial (20 mL), PySCl (10.2 mg) in ethanol (99.9 %, 4.35 mL) was mixed with APTES (45.6 μL) and left to stir for 16 h at 350 rpm and room temperature. TEOS (4.35 mL) was added to this solution and allowed to homogenize at 350 rpm for 10 min (precursor solution). In a polypropylene beaker (250 mL, diameter = 70 mm), which was equipped with a magnetic stir bar (length = 47 mm), a solution of ultrapure water (20 mL), ethanol (98 %, 190 mL) and aqueous ammonia (28–30 %, 0.1 mL) was prepared, covered with a watch glass, and left to stir at 350 rpm for 10 min (hydrolysis solution). After 10 min, the stirring speed of the hydrolysis solution was increased to 500 rpm and the

precursor solution was added quickly (< 3 s). The polypropylene beaker was covered with a watch glass and the mixture was stirred for 96 h at room temperature and 500 rpm. After the reaction time, the resulting suspension was transferred to two Falcon tubes (50 mL) and centrifuged at 4000 rpm for 10 min. The particles were washed with water (three times 20 mL per Falcon tube) and ethanol (six times 20 mL). The product was oven-dried at 80 °C for 16 h.

2.6. Variation of the synthesis parameters

Generally, the standard method for the synthesis of co-condensed Stöber particles was employed (Chapter 2.4, sample 1). Ammonia/TEOS molar ratios of 1.76, 6.15 and 16.3 were used (4 h and 96 h reaction time). Furthermore, molar ratios of water to ethanol (W/E) ranging from 0.34 to 7.27 were investigated (see Tab. S2). To evaluate the influence of the temperature, reactions were carried out at 0, 20, 40, 60 and 75 °C. The effect of the solvent was studied by replacing ethanol with butanol, 1-propanol, 2-propanol, methanol, and acetone. Finally, the silane precursor solutions were varied. APTES (84.1 µL) was replaced by APTMS (60.0 µL), TEOS (8 mL) by TMOS (5.37 mL), and ethanol (50 mL) by methanol (50 mL).

2.7. Characterization

Scanning electron microscopy (SEM) images were acquired with a Thermo Scientific Quanta FEG 250. The samples were prepared by dispersing ca. 0.2 mg of the respective particles in 1 mL of ethanol and subsequent ultrasonic treatment for 90 min. A volume of 5 µL of this dispersion was applied to the sample holder and allowed to dry for 15 min. The particle diameter was determined by measuring at least 100 particles. The uncertainty of the particle diameter refers to the standard deviation (68 %). Detailed results are given in Tab. S3. Fluorescence measurements were performed on a Perkin Elmer LS 55. Emission spectra were obtained at an excitation wavelength of 350 nm and an emission wavelength range of 360–600 nm with a resolution of 1 nm, scan speed of 240 nm·min^{-1} and an average of 10 scans. Excitation and emission slits were set to 2.5 nm. The sample (approx. 4.5 mg) was weighed into an Eppendorf tube (1.5 mL) and mixed with DMSO or cyclohexane (1 mL). This suspension was treated in an ultrasonic bath for at least 30 min. DMSO or cyclohexane (2 mL) was added to a fluorescence cuvette (d = 10 mm), 15 µL of the suspension was added, homogenized, and measured immediately. To evaluate the excimer intensity ($I_{Excimer}$), the fluorescence spectra were normalized to peak I (380 nm) and the intensity at 483 nm was determined. The following procedure was used to evaluate the accessibility of the pyrene units. Fluorescence spectra in DMSO and in cyclohexane were recorded independently from the same sample. Subsequently, the ratio of peak I and peak V was calculated for the two solvents and the difference between the two ratios was determined. This difference can be interpreted as a measure of the accessibility [46]. A large difference indicates that the pyrene units are in contact with the solvents. Nitrogen sorption isotherms were measured at 77 K with a Quantachrome Autosorb iQ MP. All samples were vacuum-degassed at 80 °C for 24 h prior to the sorption measurements. The specific surface area (SSA) was determined from the adsorption branch by a non-local density functional theory (NLDFT) model developed for silica exhibiting cylindrical pore geometry (Software ASiQwin v5.21, Quantachrome Instruments, Boynton Beach, FL, USA). The total pore volume (V_p) was calculated from the amount of adsorbed nitrogen at a relative pressure of ca. 0.95. The micropore volume (V_{micro}) was determined using the α_s method. Adsorption isotherms are given in Fig. S4.

3. Results and discussion

3.1. Co-condensation of PySCl-APTES

First, the ideal amounts of APTES and PySCl for the co-condensation had to be determined (see Tab. S1 for the different amounts that were used). For this purpose, the synthesis of Stöber-type silica particles according to Gallagher *et al.* [45] was carried out and the product was analyzed by nitrogen sorption. The results indicated the presence of porous particles, with a total pore volume of 0.148 cm^3·g^{-1}, a micropore volume of 0.074 cm^3·g^{-1}, and a SSA of 376 m^2·g^{-1}. The particle diameter was 330 ± 17 nm. Due to the high porosity, it was concluded that a growth mechanism by aggregation had occurred under these conditions [11–13]. It could therefore be expected that the incorporation of pyrene units via the co-condensation of PySCl-APTES would lead to an excimer band in the fluorescence spectrum of the resulting particles. We thus determined the amounts of APTES and PySCl required for excimer formation with the aim of keeping these quantities as low as possible so as not to influence the mechanism of particle growth. First, APTES was co-condensed in a wide range of quantities relative to the amount of TEOS (molar ratio of APTES/TEOS = 10^{-7} to 0.25) and the influence on the particle size and porosity was investigated. There was no significant difference in particle size in the range of 0.001 to 0.025 (APTES/TEOS, see Fig. S1). Similar values for the pore volume and the SSA as for the particles produced by Gallagher *et al.* [45] were obtained in the range of 0.001 to 0.010 (APTES/TEOS). Consequently, a range of 0.003 to 0.010 (APTES/TEOS) was chosen with an APTES/PySCl ratio of 6. The fluorescence spectra obtained for the corresponding co-condensed particles are shown in Fig. 1. It was observed that the excimer band expected for particles formed by aggregation was prominently present for samples prepared with an APTES/TEOS ratio of 0.010 (18.6 mg of APTES). It was suspected that at lower amounts of APTES and consequently of PySCl, the quantity of incorporated pyrene units was insufficient for excimer formation. In addition, a blank experiment was performed with PySCl but in the absence of APTES to show that APTES is indeed necessary to covalently anchor the pyrene units in the silica framework. As can be seen in Fig. 1(e), the corresponding particles showed no fluorescence.

3.2. Proof of concept

To demonstrate the applicability of the developed method, it must be shown that the chosen quantities of APTES and PySCl are suitable for distinguishing between growth by aggregation and by monomer addition. For this purpose, the composition of the reaction mixture was

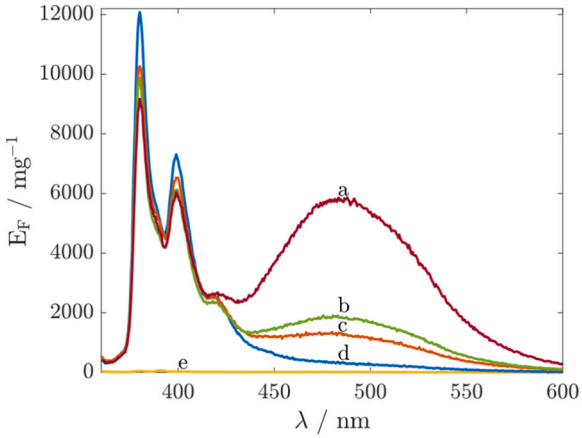

Fig. 1. Fluorescence spectra of particles prepared by co-condensation with various APTES/TEOS ratios. (a) 0.010, (b) 0.008, (c) 0.007, (d) 0.003, (e) blank experiment without APTES. A constant APTES/PySCl ratio of 6 was used. The intensity was normalized to the mass of the particles in the cuvette.

varied (Table 1).

In a first step, the volume of the hydrolysis solution was almost doubled, and the relative ammonia concentration was almost halved. As shown in Fig. 2, excimer fluorescence was still observed under these conditions (Fig. 2(b)). When the ammonia concentration was further reduced, excimer fluorescence was no longer observed (Fig. 2(c)) and the particles had a low total pore volume (0.04 $cm^3 \cdot g^{-1}$) as well as a low SSA of 18 $m^2 \cdot g^{-1}$. As expected [47], smaller particles were obtained for lower base concentrations (Fig. 3). The results support the hypothesis that particle growth under the conditions with lower base concentration occurred by monomer addition. As shown later, monomer addition was also observed when studying the influence of the water content, temperature, and solvent.

3.3. Influence of the base concentration and reaction time

Different reaction times were chosen to evaluate whether the growth mechanism was the same throughout the reaction. It was found that the relative excimer intensity increased with increasing base concentration given a reaction time of 4 h (Table 2). Interestingly, a decrease of the excimer intensity was observed after 96 h for the samples with a molar equivalent of ammonia to TEOS of 6.15 and 16.3. This indicates that an aggregation mechanism prevails in the first few hours of the reaction, changing towards monomer addition at a later stage. This effect was more pronounced at higher base concentrations, most likely because the reaction proceeds at a faster rate under these conditions [48].

To further investigate the observed trend, the particles were analyzed by nitrogen sorption. For a given composition of the reaction mixture, the micropore volume was smaller after 96 h than after 4 h (Table 2), thus supporting the hypothesis of an initial growth by aggregation, which changes over time towards growth by monomer addition and ultimately leads to a partial sealing of the micropores.

3.4. Influence of the water/ethanol ratio

To exclude possible dilution effects, the volume of the reaction mixture was kept constant when varying the water/ethanol ratio. The excimer intensities obtained for the resulting particles are shown in Fig. 4. Up to a molar water/ethanol ratio (W/E) of 2.60, the intensity of the excimer band was small, indicating growth by monomer addition. However, a strong increase of the excimer band intensity was observed in the range of 2.60 to 4.15, most likely due to an increased contribution of the growth by aggregation mechanism. An influence of hydrophobic interaction-driven pyrene dimerization on the growth mechanism in water-rich environments cannot be completely ruled out, although excimer formation of negatively charged pyrene derivatives is only observed in water at concentrations above 1 mM. Furthermore, the presence of a slightly less polar solvent was found to dramatically decrease the tendency towards pyrene dimerization [49].

The excimer intensity correlates well with the accessibility and the pore volume (Fig. 5). It was concluded from these results that at a low W/E ratio, particle growth mainly occurs via monomer addition, leading to a low excimer intensity, low total pore and micropore volume, low SSA as well as a low accessibility of the incorporated pyrene units for solvents of different polarity. At a W/E ratio above 2.6, growth by aggregation is dominant, leading to porous particles with accessible pyrene units.

Table 1
Particles were synthesized with different compositions of the reaction mixture. In all cases, the APTES/TEOS ratio was set to 0.010 and the APTES/PySCl ratio to 6. The numbers correspond to the molar equivalents relative to TEOS.

	TEOS	APTES	PySCl	ethanol	water	ammonia
sample 1	1.00	0.010	0.0017	24	81	6.15
sample 2	1.00	0.010	0.0017	170	56	3.23
sample 3	1.00	0.010	0.0017	170	56	0.08

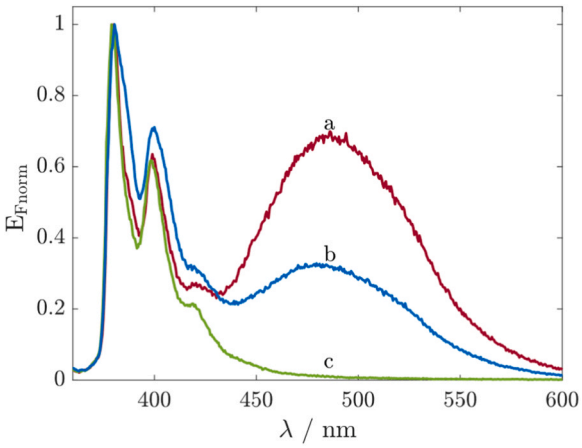

Fig. 2. Normalized (peak I) fluorescence spectra of (a) sample 1, (b) sample 2, and (c) sample 3. Refer to Table 1 for the respective composition of the reaction mixture.

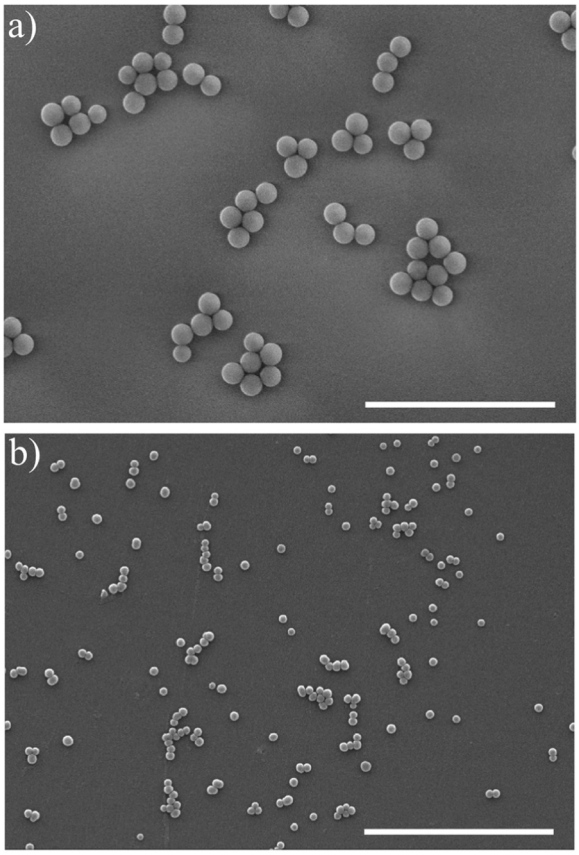

Fig. 3. SEM images of (a) sample 1 and (b) sample 3. Refer to Table 1 for the respective composition of the reaction mixture. The scale bar is 3 μm in both images.

The results shown in Fig. 5 can be explained by adopting a kinetic approach previously proposed for the hydrolysis of TEOS (Eq. (1)) [47]. As we have kept the concentrations of TEOS and ammonia constant in our experiments, the rate of hydrolysis of TEOS only depends on the concentration of water. Faster hydrolysis of TEOS is therefore expected with increasing water concentrations, i.e., with increasing W/E ratio.

Table 2
Excimer intensity ($I_{Excimer}$) and micropore volume (V_{micro}) as a function of base concentration and reaction time. In all cases, the APTES/TEOS ratio was set to 0.010 and the APTES/PySCl ratio to 6. The numbers in the solvent columns correspond to the respective molar equivalents relative to TEOS.

Ethanol	Water	Ammonia	Time/h	$I_{Excimer}$	$V_{micro}/cm^3 \cdot g^{-1}$
24	81	1.76	4	0.48	0.085
24	81	1.76	96	1.05	0.067
24	81	6.15	4	0.64	0.091
24	81	6.15	96	0.61	0.073
24	81	16.3	4	0.83	0.093
24	81	16.3	96	0.40	0.063

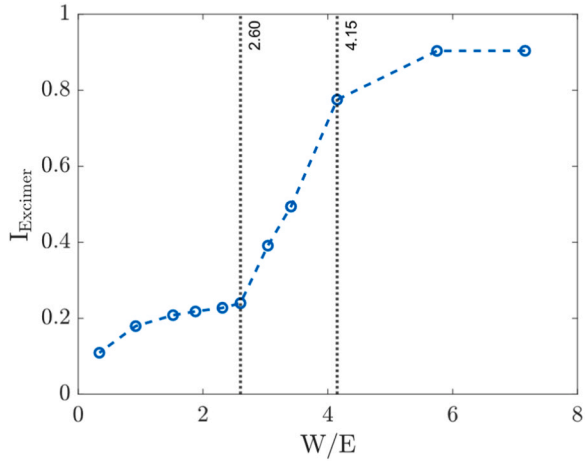

Fig. 4. $I_{Excimer}$ as a function of the molar water/ethanol ratio (W/E, 4 h of reaction time). In all cases, the APTES/TEOS ratio was set to 0.010 and the APTES/PySCl ratio to 6. The ammonia/TEOS ratio was 6.15. The volume of the reaction mixture was identical for all experiments.

$$\frac{d[\mathrm{TEOS}]}{dt} = -k_H \cdot [H_2O]^{1.5} \cdot [NH_3]^{0.5} \cdot [\mathrm{TEOS}] \quad (1)$$

The results indicate that at a W/E ratio above 2.60, aggregation is the predominant growth mechanism. It can be assumed that a certain hydrolysis rate must be present to achieve the highest possible concentration of condensable intermediates to form primary particles. Under slow hydrolysis conditions (low W/E ratio), on the other hand, the low concentration of condensable intermediates results in a low probability of cross-linking, making a growth by monomer addition more likely. To ensure that these results were not influenced by APTES and PySCl, particles were prepared under the same conditions but without APTES and PySCl (see Fig. S2), leading to the conclusion that the co-condensation of PySCl-APTES indeed does not have a significant effect on the structural properties of the resulting particles under the conditions investigated in this work.

To explain why the plot of the excimer intensity against the W/E ratio does not show such a pronounced step as observed in the respective plots of the accessibility and the pore volume (Fig. 5), time-resolved experiments were carried out. A sample (3 mL) was taken at specific time intervals during the particle growth and placed in ethanol (10 mL) to quench the reaction. Three conditions were investigated: low water content (W/E = 0.92), intermediate water content (W/E = 3.38), and high water content (W/E = 7.27). Based on the results reported in Fig. 6, we can expect a mechanism predominantly based on monomer addition for W/E = 0.92, whereas particle growth at W/E = 7.27 mainly proceeds by aggregation. The intermediate water content was selected due to the discrepancy between the comparatively low excimer intensity and the large total pore volume of the resulting particles (0.149 $cm^3 \cdot g^{-1}$). It seems that under the conditions of intermediate water content, particle growth follows a mixed mechanism that leads to porous particles while still providing a certain degree of spatial separation between the incorporated pyrene units. To check whether the hypothesis of a mixed mechanism is valid, the evolution of the growth mechanism was investigated over the course of the reaction.

In the case of high water content, a strong increase of the excimer intensity was observed between 10 min and 180 min. This indicates that during the first 180 min, growth by aggregation is the predominant mechanism. In contrast, the experiment conducted at low water content showed only a small increase of the excimer intensity over the entire period of 240 min, indicating growth by monomer addition. Interestingly, the experiment performed at intermediate water content featured an unusual development of the excimer intensity over the course of the reaction. The small initial slope points to growth by monomer addition in the early stages of the reaction. However, after 120 min, the pronounced increase of the excimer intensity indicates a more complex mechanism, with growth by aggregation becoming more prevalent. Similar to the experiment at high water content, the excimer intensity levelled off after 180 min.

To gain a better understanding of the underlying growth mechanism, the particle sizes for low, intermediate, and high water content were determined. It was found that in all cases the particles became continuously larger during the reaction. As an example, this is illustrated for the intermediate water content in Fig. 7.

Three different regimes were identified for the growth under the conditions of intermediate water content, as illustrated by the slopes of the respective linear fits to the $I_{Excimer}$ versus time plot (Table 3). Assuming growth by monomer addition for low water content and growth by aggregation for high water content, the slopes for intermediate water content can be expressed as a linear combination of these two general mechanisms. However, it should be mentioned that the assumption of an exclusive growth by monomer addition or aggregation, respectively, is a simplification.

At an intermediate water content, the initial stage of the particle growth proceeds predominantly by monomer addition, leading to a low excimer intensity. Between 120 and 180 min, the reaction follows a mixed mechanism, where aggregation considerably contributes to particle growth and produces the observed pore volume of the final product. Interestingly, the porosity is conserved although the later stages of the particle growth are again dominated by monomer addition.

3.5. Influence of the temperature

The influence of the reaction temperature was investigated under the conditions used for the synthesis of sample 1 (Table 1). The excimer intensities and total pore volumes of the resulting particles are shown in Fig. 8. As expected, the excimer intensity increases with increasing reaction temperature up to 60 °C. A slight decrease of the excimer intensity was observed at 75 °C. This could indicate that the efficient growth by aggregation caused by the fast hydrolysis of TEOS at elevated temperatures [50] quickly reduces the concentration of condensable precursors, thus leading to monomer growth during the late stages of the reaction. From the data shown in Fig. 8 it can be concluded that particle growth at 0 °C proceeds mainly by monomer addition, whereas growth by aggregation is the predominant mechanism at 60 °C, evidenced by the much larger total pore volume and higher excimer intensity.

3.6. Influence of the solvent and silica precursor

The experiments were conducted according to the synthesis of sample 1 (Table 1). Instead of ethanol, an identical volume of 1-butanol, 1-propanol, 2-propanol, methanol, or acetone was used. Particles obtained with 1-butanol and 1-propanol were non-spherical. These solvents were therefore not further considered. Particles obtained with 2-propanol had a relatively low excimer intensity indicative of growth by monomer addition. With methanol, particles exhibited about 18 %

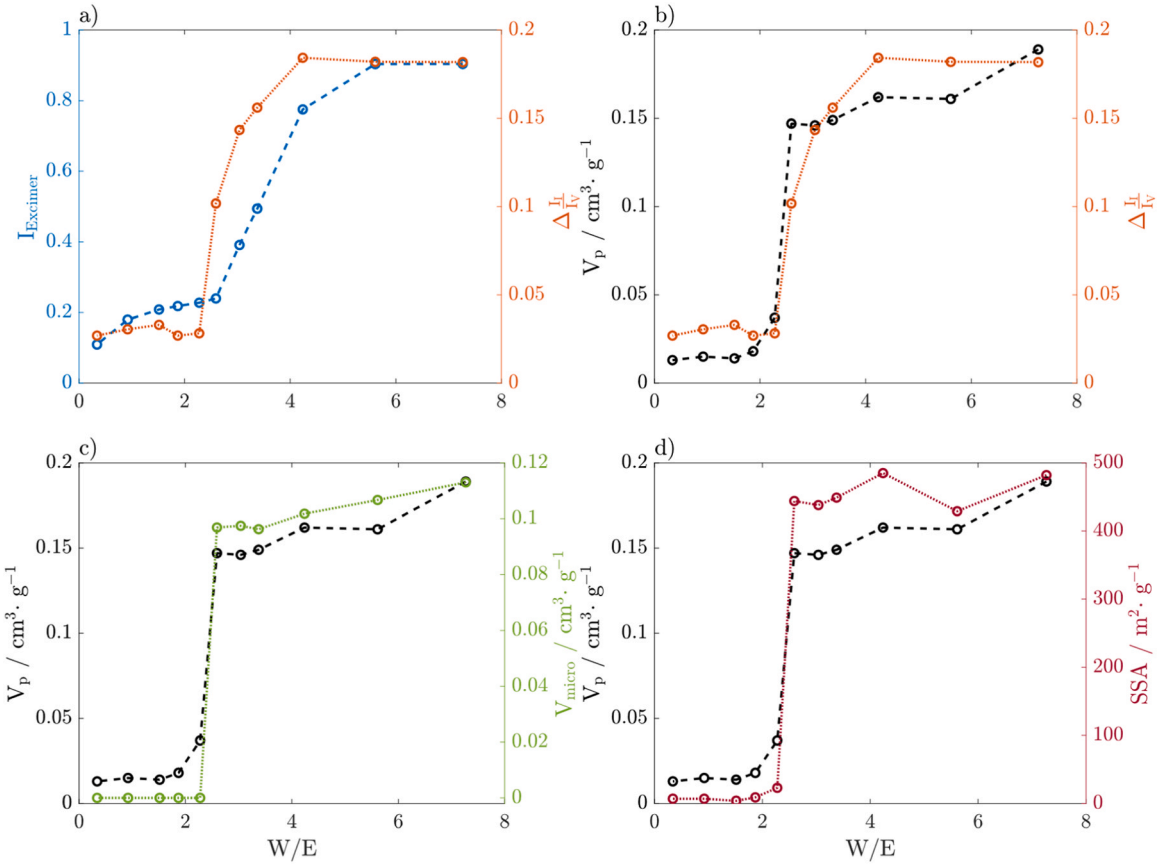

Fig. 5. (a) $I_{Excimer}$ (blue, dashed) and accessibility (orange, dotted), (b) total pore volume (black, dashed) and accessibility (orange, dotted), (c) total pore volume (black, dashed) and micropore volume (green, dotted), and (d) total pore volume (black, dashed) and SSA (red, dotted) as a function of the water/ethanol ratio.

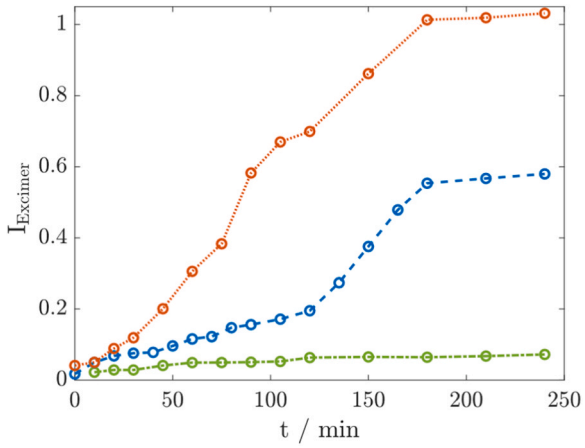

Fig. 6. $I_{Excimer}$ as a function of time for particle growth conducted at various water/ethanol ratios: high (W/E = 7.27, orange, dotted), intermediate (W/E = 3.38, blue, dashed), and low (W/E = 0.92, green, dash-dotted). The corresponding fluorescence spectra are given in Fig. S3.

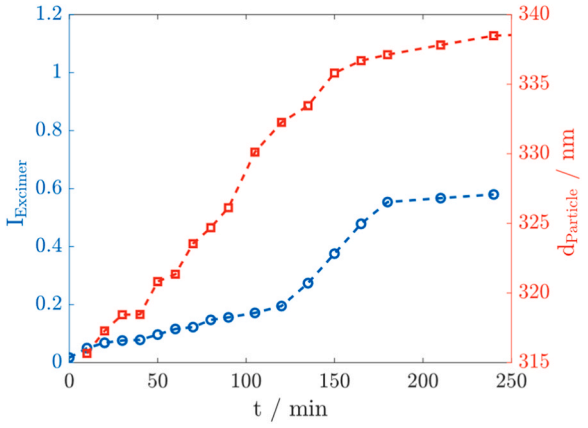

Fig. 7. $I_{Excimer}$ (blue circles) and particle diameter (red squares) plotted against time for particle growth under intermediate water content.

higher excimer intensity compared to the particles obtained by means of the classical synthesis with ethanol. With acetone, particles featured an extraordinarily high excimer intensity (Table 4). The back reaction of the TEOS hydrolysis is suppressed when using acetone. We can thus expect high concentrations of hydrolyzed precursors in acetone that promote efficient cross-linking and consequently particle growth by aggregation.

For the alcoholic solvents, the excimer intensity was found to be inversely proportional to the molar mass. Our results so far suggest an

Table 3
Slope of the linear fit to the $I_{Excimer}$ versus time plot and description of the mechanism by a linear combination assuming particle growth exclusively by monomer addition (at low water content, 100 % monomer) and aggregation (at high water content, 100 % aggregation).

water content	slope·10^2/min^{-1}	monomer/%	aggregation/%	time/min
low	0.021	100	0	10–120
intermediate	0.082	90	10	0–120
intermediate	0.369	40	60	120–180
intermediate	0.026	99	1	180–240
high	0.603	0	100	10–180

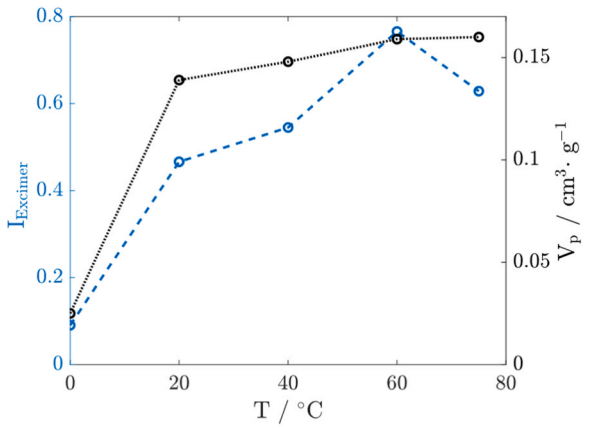

Fig. 8. $I_{Excimer}$ (blue, dashed) and total pore volume (black, dotted) for particles obtained at different temperatures.

Table 4
$I_{Excimer}$ for particles obtained under the conditions used for the synthesis of sample 1 with various solvents (identical volumes).

solvent	$I_{Excimer}$
2-propanol	0.13
ethanol	0.49
methanol	0.58
acetone	2.87

influence of the hydrolysis rate on the growth mechanism. Table 5 summarizes the conclusions from literature regarding hydrolysis rates in the synthesis of silica particles with different solvents. There is a good agreement between the excimer intensity and the hydrolysis rate observed in the respective solvent, with fast hydrolysis leading to growth by aggregation and thus to a high excimer intensity. Only Bari *et al.* [50] proposed a reverse order, mentioning that the differences between the individual publications can be explained by different analytical methods and their uncertainties [50].

It is well-known that the hydrolysis of TMOS is faster than the hydrolysis of TEOS under otherwise identical conditions [47]. We would therefore expect a higher excimer intensity for particles synthesized with TMOS. Following the procedure for the synthesis of sample 1 but replacing TEOS with TMOS, APTES with APTMS, and ethanol with methanol resulted in particles with $I_{Excimer} = 0.82$ (compared to $I_{Excimer} = 0.49$ for particles obtained with TEOS). This is further evidence that the growth mechanism largely depends on the hydrolysis rate.

4. Conclusions

In this work, a method was developed to monitor the growth mechanism of silica particles using pyrene as a fluorescent probe. The experiments indicate that the growth mechanism is determined by the rate of hydrolysis. Fast hydrolysis leads to a fast growth by aggregation, which results in a high intensity of the pyrene excimer emission. The resulting particles are porous with pyrene moieties that are accessible to solvent molecules. Under the conditions of slow hydrolysis, growth by monomer addition is the predominant mechanism. In this case the particles are essentially non-porous with inaccessible pyrene moieties. In terms of the reaction conditions, a high base concentration, high water content and high reaction temperature favor growth by aggregation. The results confirm previous observations of porous structures resulting from fast growth rates and dense non-porous frameworks being formed under conditions that cause slow particle growth [54–56]. Based on these results, we expect that the concept of probing the growth mechanism through the co-condensation of PySCl-APTES conjugates can

Table 5
Order of the hydrolysis rate in silica particle growth conducted in the presence of various alcohols.

hydrolysis rate	Refs.
methanol > ethanol > 2-propanol	[47,51,52]
ethanol > 2-propanol	[53]
2-propanol > ethanol	[50]

provide information on a wide variety of silicate-based systems, including mesoporous silica prepared via a direct synthesis pathway [57,58] or by pseudomorphic transformation [59–61], as well as on sol-gel derived bioglass scaffolds [62,63].

CRediT authorship contribution statement

Dominik Brühwiler: Writing – review & editing, Writing – original draft, Visualization, Validation, Supervision, Resources, Project administration, Methodology, Investigation, Funding acquisition, Formal analysis, Data curation, Conceptualization. **Fabian Walther:** Writing – review & editing, Writing – original draft, Visualization, Validation, Methodology, Investigation, Formal analysis, Data curation, Conceptualization.

Declaration of Competing Interest

The authors declare that they have no known competing financial interests or personal relationships that could have appeared to influence the work reported in this paper.

Data availability

Data will be made available on request.

Acknowledgements

This research did not receive any specific grant from funding agencies in the public, commercial, or not-for-profit sectors. Financial support was provided by the ZHAW Zurich University of Applied Sciences.

Appendix A. Supporting information

Supplementary data associated with this article can be found in the online version at doi:10.1016/j.colsurfa.2024.133234.

References

[1] W. Stöber, A. Fink, E. Bohn, Controlled growth of monodisperse silica spheres in the micron size range, J. Colloid Interface Sci. 26 (1968) 62–69, https://doi.org/10.1016/0021-9797(68)90272-5.
[2] N. Plumeré, B. Speiser, H.A. Mayer, D. Joosten, L. Wesemann, High-temperature chlorination-reduction sequence for the preparation of silicon hydride modified silica surfaces, Chem. - Eur. J. 15 (2009) 936–946, https://doi.org/10.1002/chem.200801213.
[3] M.H. Lee, F.L. Beyer, E.M. Furst, Synthesis of monodisperse fluorescent core-shell silica particles using a modified Stöber method for imaging individual particles in dense colloidal suspensions, J. Colloid Interface Sci. 288 (2005) 114–123, https://doi.org/10.1016/j.jcis.2005.02.073.
[4] C. Chen, Y. Li, S. Liu, Fabrication of macroporous platinum using monodisperse silica nanoparticle template and its application in methanol catalytic oxidation, J. Electroanal. Chem. 632 (2009) 14–19, https://doi.org/10.1016/j.jelechem.2009.03.009.
[5] L. Huang, M. Liu, L. Mao, D. Xu, Q. Wan, G. Zeng, Y. Shi, Y. Wen, X. Zhang, Y. Wei, Preparation and controlled drug delivery applications of mesoporous silica polymer nanocomposites through the visible light induced surface-initiated ATRP, Appl. Surf. Sci. 412 (2017) 571–577, https://doi.org/10.1016/j.apsusc.2017.04.026.
[6] Y.-J. Kim, H.-S. Jung, J. Lim, S.-J. Ryu, J.-K. Lee, Rapid imaging of latent fingerprints using biocompatible fluorescent silica nanoparticles, Langmuir 32 (2016) 8077–8083, https://doi.org/10.1021/acs.langmuir.6b01977.

[7] R.S. Fernandes, I.M. Raimundo, M.F. Pimentel, Revising the synthesis of Stöber silica nanoparticles: a multivariate assessment study on the effects of reaction parameters on the particle size, Colloids Surf. Physicochem. Eng. Asp. 577 (2019) 1–7, https://doi.org/10.1016/j.colsurfa.2019.05.053.
[8] T. Matsoukas, E. Gulari, Dynamics of growth of silica particles from ammonia-catalyzed hydrolysis of tetra-ethyl-orthosilicate, J. Colloid Interface Sci. 124 (1988) 252–261, https://doi.org/10.1016/0021-9797(88)90346-3.
[9] T. Matsoukas, E. Gulari, Monomer-addition growth with a slow initiation step: A growth model for silica particles from alkoxides, J. Colloid Interface Sci. 132 (1989) 13–21, https://doi.org/10.1016/0021-9797(89)90210-5.
[10] A. Van Blaaderen, J. Van Geest, A. Vrij, Monodisperse colloidal silica spheres from tetraalkoxysilanes: particle formation and growth mechanism, J. Colloid Interface Sci. 154 (1992) 481–501, https://doi.org/10.1016/0021-9797(92)90163-G.
[11] G.H. Bogush, C.F. Zukoski, Studies of the kinetics of the precipitation of uniform silica particles through the hydrolysis and condensation of silicon alkoxides, J. Colloid Interface Sci. 142 (1991) 1–18, https://doi.org/10.1016/0021-9797(91)90029-8.
[12] G.H. Bogush, C.F. Zukoski, Uniform silica particle precipitation: an aggregative growth model, J. Colloid Interface Sci. 142 (1991) 19–34, https://doi.org/10.1016/0021-9797(91)90030-C.
[13] H. Giesche, Synthesis of monodispersed silica powders I. Particle properties and reaction kinetics, J. Eur. Ceram. Soc. 14 (1994) 189–204, https://doi.org/10.1016/0955-2219(94)90087-6.
[14] S. Li, Q. Wan, Z. Qin, Y. Fu, Y. Gu, Understanding Stöber silica's pore characteristics measured by gas adsorption, Langmuir 31 (2015) 824–832, https://doi.org/10.1021/la5042103.
[15] S. Li, Q. Wan, Z. Qin, Y. Fu, Y. Gu, Unraveling the mystery of Stöber silica's microporosity, Langmuir 32 (2016) 9180–9187, https://doi.org/10.1021/acs.langmuir.6b02472.
[16] J. Luo, W. Chu, S. Sall, C. Petit, Facile synthesis of monodispersed Au nanoparticles-coated on Stöber silica, Colloids Surf. Physicochem. Eng. Asp. 425 (2013) 83–91, https://doi.org/10.1016/j.colsurfa.2013.02.056.
[17] J.M. Kim, S.M. Chang, S.M. Kong, K.-S. Kim, J. Kim, W.-S. Kim, Control of hydroxyl group content in silica particle synthesized by the sol-precipitation process, Ceram. Int. 35 (2009) 1015–1019, https://doi.org/10.1016/j.ceramint.2008.04.011.
[18] L. Peng, W. Qisui, L. Xi, Z. Chaocan, Investigation of the states of water and OH groups on the surface of silica, Colloids Surf. Physicochem. Eng. Asp. 334 (2009) 112–115, https://doi.org/10.1016/j.colsurfa.2008.10.028.
[19] R. Filipović, Z. Obrenović, I. Stijepović, L.M. Nikolić, V.V. Srdić, Synthesis of mesoporous silica particles with controlled pore structure, Ceram. Int. 35 (2009) 3347–3353, https://doi.org/10.1016/j.ceramint.2009.05.040.
[20] F. Balas, M. Rodríguez-Delgado, C. Otero-Arean, F. Conde, E. Matesanz, L. Esquivias, J. Ramírez-Castellanos, J. Gonzalez-Calbet, M. Vallet-Regí, Structural characterization of nanosized silica spheres, Solid State Sci. 9 (2007) 351–356, https://doi.org/10.1016/j.solidstatesciences.2007.03.004.
[21] A.G. Howard, N.H. Khdary, Spray synthesis of monodisperse sub-micron spherical silica particles, Mater. Lett. 61 (2007) 1951–1954, https://doi.org/10.1016/j.matlet.2006.07.110.
[22] I. Dekany, J. Nemeth, M. Szekeres, R. Schoonheydt, Surfacial, liquid sorption and monolayer-forming properties of hydrophilic and hydrophobic Stöber silica particles, Colloid Polym. Sci. 282 (2003) 1–6, https://doi.org/10.1007/s00396-003-0930-1.
[23] M. Szekeres, J. Tóth, I. Dékány, Specific surface area of stoeber silica determined by various experimental methods, Langmuir 18 (2002) 2678–2685, https://doi.org/10.1021/la011370j.
[24] A. Labrosse, A. Burneau, Characterization of porosity of ammonia catalysed alkoxysilane silica, J. Non-Cryst. Solids 221 (1997) 107–124, https://doi.org/10.1016/S0022-3093(97)00414-6.
[25] P.J. Davis, R. Deshpande, D.M. Smith, C.J. Brinker, R.A. Assink, Pore structure evolution in silica gel during aging/drying. IV. Varying pore fluid pH, J. Non-Cryst. Solids 167 (1994) 295–306, https://doi.org/10.1016/0022-3093(94)90252-6.
[26] A. van Blaaderen, A. Vrij, Synthesis and characterization of monodisperse colloidal organo-silica spheres, J. Colloid Interface Sci. 156 (1993) 1–18, https://doi.org/10.1006/jcis.1993.1073.
[27] A.J. Lecloux, J. Bronckart, F. Noville, C. Dodet, P. Marchot, J.P. Pirard, Study of the texture of monodisperse silica sphere samples in the nanometer size range, Colloids Surf. 19 (1986) 359–374, https://doi.org/10.1016/0166-6622(86)80289-X.
[28] C.C.M.C. Carcouët, M.W.P. van de Put, B. Mezari, P.C.M.M. Magusin, J. Laven, P.H. H. Bomans, H. Friedrich, A.C.C. Esteves, N.A.J.M. Sommerdijk, R.A.T.M. van Benthem, G. de With, Nucleation and Growth of Monodisperse Silica Nanoparticles, Nano Lett. 14 (2014) 1433–1438, https://doi.org/10.1021/nl404550d.
[29] J.K. Bailey, M.L. Mecartney, Formation of colloidal silica particles from alkoxides, Colloids Surf. 63 (1992) 151–161, https://doi.org/10.1016/0166-6622(92)80081-C.
[30] G.H. Bogush, M.A. Tracy, C.F. Zukoski, Preparation of monodisperse silica particles: control of size and mass fraction, J. Non-Cryst. Solids 104 (1988) 95–106, https://doi.org/10.1016/0022-3093(88)90187-1.
[31] C.J. Brinker, K.D. Keefer, D.W. Schaefer, R.A. Assink, B.D. Kay, C.S. Ashley, Sol-gel transition in simple silicates II, J. Non-Cryst. Solids 63 (1984) 45–59, https://doi.org/10.1016/0022-3093(84)90385-5.
[32] C.H. Lochmuller, A.S. Colborn, M.L. Hunnicutt, J.M. Harris, Bound pyrene excimer photophysics and the organization and distribution of reaction sites on silica, J. Am. Chem. Soc. 106 (1984) 4077–4082, https://doi.org/10.1021/ja00327a002.
[33] J. Seixas de Melo, T. Costa, M. da G. Miguel, B. Lindman, K. Schillén, Time-resolved and steady-state fluorescence studies of hydrophobically modified water-soluble polymers, J. Phys. Chem. B. 107 (2003) 12605–12621, https://doi.org/10.1021/jp0346054.
[34] P. Conlon, C.J. Yang, Y. Wu, Y. Chen, K. Martinez, Y. Kim, N. Stevens, A.A. Marti, S. Jockusch, N.J. Turro, W. Tan, Pyrene excimer signaling molecular beacons for probing nucleic acids, J. Am. Chem. Soc. 130 (2008) 336–342, https://doi.org/10.1021/ja076411y.
[35] R.D. Pensack, R.J. Ashmore, A.L. Paoletta, G.D. Scholes, The nature of excimer formation in crystalline pyrene nanoparticles, J. Phys. Chem. C. 122 (2018) 21004–21017, https://doi.org/10.1021/acs.jpcc.8b03963.
[36] G.K. Bains, S.H. Kim, E.J. Sorin, V. Narayanaswami, The extent of pyrene excimer fluorescence emission is a reflector of distance and flexibility: analysis of the segment linking the LDL receptor-binding and tetramerization domains of apolipoprotein E3, Biochemistry 51 (2012) 6207–6219, https://doi.org/10.1021/bi3005285.
[37] O. Taratula, J. Rochford, P. Piotrowiak, E. Galoppini, R.A. Carlisle, G.J. Meyer, Pyrene-terminated phenylenethynylene rigid linkers anchored to metal oxide nanoparticles, J. Phys. Chem. B. 110 (2006) 15734–15741, https://doi.org/10.1021/jp0623847.
[38] J.C. Hicks, C.W. Jones, Controlling the density of amine sites on silica surfaces using benzyl spacers, Langmuir 22 (2006) 2676–2681, https://doi.org/10.1021/la053024y.
[39] M. Mazur, G.J. Blanchard, Probing intermolecular communication with surface-attached pyrene, J. Phys. Chem. B 109 (2005) 4076–4083, https://doi.org/10.1021/jp045323m.
[40] P.P. Ghimire, M. Jaroniec, Renaissance of Stöber method for synthesis of colloidal particles: New developments and opportunities, J. Colloid Interface Sci. 584 (2021) 838–865, https://doi.org/10.1016/j.jcis.2020.10.014.
[41] P.J. Dewar, T.F. MacGillivray, S.M. Crispo, T. Smith-Palmer, Interactions of pyrene-labeled silica particles, J. Colloid Interface Sci. 228 (2000) 253–258, https://doi.org/10.1006/jcis.2000.6937.
[42] K. Kalyanasundaram, J.K. Thomas, Environmental effects on vibronic band intensities in pyrene monomer fluorescence and their application in studies of micellar systems, J. Am. Chem. Soc. 99 (1977) 2039–2044, https://doi.org/10.1021/ja00449a004.
[43] M. Hemgesberg, S. Schütz, C. Müller, M. Schlörholz, H. Latzel, Y. Sun, C. Ziegler, W.R. Thiel, Ultra-fast photo-patterning of hydroxamic acid layers adsorbed on TiAlN: the challenge of modeling thermally induced desorption, Appl. Surf. Sci. 259 (2012) 406–415, https://doi.org/10.1016/j.apsusc.2012.07.059.
[44] J.B. Issa, A.S. Salameh, E.W. Castner, J.F. Wishart, S.S. Isied, Conformational analysis of the electron-transfer kinetics across oligoproline peptides using *N,N* -Dimethyl-1,4-benzenediamine donors and pyrene-1-sulfonyl acceptors, J. Phys. Chem. B 111 (2007) 6878–6886, https://doi.org/10.1021/jp071599t.
[45] S.H. Gallagher, P. Schlauri, E. Cesari, J. Durrer, D. Brühwiler, Silica particles with fluorescein-labelled cores for evaluating accessibility through fluorescence quenching by copper, Nanoscale Adv. 3 (2021) 6459–6467, https://doi.org/10.1039/D1NA00599E.
[46] J. González-Benito, A.J. Aznar, J. Lima, F. Bahia, A.L. Maçanita, J. Baselga, Fluorescence-labeled pyrenesulfonamide response for characterizing polymeric interfaces in composite materials, J. Fluor. 10 (2000), https://doi.org/10.1023/A:1009491009039, 141–141.
[47] M.T. Harris, R.R. Brunson, C.H. Byers, The base-catalyzed hydrolysis and condensation reactions of dilute and concentrated TEOS solutions, J. Non-Cryst. Solids 121 (1990) 397–403, https://doi.org/10.1016/0022-3093(90)90165-I.
[48] K. Lee, J.-L. Look, M.T. Harris, A.V. McCormick, Assessing extreme models of the stöber synthesis using transients under a range of initial composition, J. Colloid Interface Sci. 194 (1997) 78–88, https://doi.org/10.1006/jcis.1997.5089.
[49] G. Jones, V.I. Vullev, Ground- and excited-state aggregation properties of a pyrene derivative in aqueous media, J. Phys. Chem. A. 105 (2001) 6402–6406, https://doi.org/10.1021/jp010087q.
[50] A.H. Bari, R.B. Jundale, AmolA. Kulkarni, Understanding the role of solvent properties on reaction kinetics for synthesis of silica nanoparticles, Chem. Eng. J. 398 (2020) 125427, https://doi.org/10.1016/j.cej.2020.125427.
[51] S. Sadasivan, A.K. Dubey, Y. Li, D.H. Rasmussen, Alcoholic solvent effect on silica synthesis—NMR and DLS investigation, J. Sol. -Gel Sci. Technol. 12 (1998) 5–14, https://doi.org/10.1023/A:1008659708390.
[52] O. Malay, I. Yilgor, Y.Z. Menceloglu, Effects of solvent on TEOS hydrolysis kinetics and silica particle size under basic conditions, J. Sol-Gel Sci. Technol. 67 (2013) 351–361, https://doi.org/10.1007/s10971-013-3088-4.
[53] D.R. Hristov, E. Mahon, K.A. Dawson, Controlling aqueous silica nanoparticle synthesis in the 10–100 nm range, Chem. Commun. 51 (2015) 17420–17423, https://doi.org/10.1039/C5CC06598D.
[54] L. Jelinek, P. Dong, C. Rojas-Pazos, H. Taibi, E. Kovats, Study of the Stöber reaction. Properties of colloidal silica spheres prepared via alkoxide hydrolysis, Langmuir 8 (1992) 2152–2164, https://doi.org/10.1021/la00045a015.
[55] H. Boukari, J.S. Lin, M.T. Harris, Probing the dynamics of the silica nanostructure formation and growth by SAXS, Chem. Mater. 9 (1997) 2376–2384, https://doi.org/10.1021/cm9702878.
[56] H. Boukari, J.S. Lin, M.T. Harris, Small-Angle X-Ray scattering study of the formation of colloidal silica particles from alkoxides: primary particles or not? J. Colloid Interface Sci. 194 (1997) 311–318, https://doi.org/10.1006/jcis.1997.5112.
[57] C.T. Kresge, M.E. Leonowicz, W.J. Roth, J.C. Vartuli, J.S. Beck, Ordered mesoporous molecular sieves synthesized by a liquid-crystal template mechanism, Nature 359 (1992) 710–712, https://doi.org/10.1038/359710a0.
[58] D. Zhao, J. Feng, Q. Huo, N. Melosh, G.H. Fredrickson, B.F. Chmelka, G.D. Stucky, Triblock copolymer syntheses of mesoporous silica with periodic 50 to 300

angstrom pores, Science 279 (1998) 548–552, https://doi.org/10.1126/science.279.5350.548.
[59] A. Galarneau, J. Iapichella, K. Bonhomme, F. Di Renzo, P. Kooyman, O. Terasaki, F. Fajula, Controlling the morphology of mesostructured silicas by pseudomorphic transformation: a route towards applications, Adv. Funct. Mater. 16 (2006) 1657–1667, https://doi.org/10.1002/adfm.200500825.
[60] M.J. Reber, D. Brühwiler, Bimodal mesoporous silica with bottleneck pores, Dalton Trans. 44 (2015) 17960–17967, https://doi.org/10.1039/C5DT03082J.
[61] M.J. Reber, D. Brühwiler, Mesoporous hybrid materials by simultaneous pseudomorphic transformation and functionalization of silica microspheres, Part. Part. Syst. Charact. 32 (2015) 243–250, https://doi.org/10.1002/ppsc.201400150.
[62] R. Li, A.E. Clark, L.L. Hench, An investigation of bioactive glass powders by sol-gel processing, J. Appl. Biomater. 2 (1991) 231–239, https://doi.org/10.1002/jab.770020403.
[63] X. Yan, C. Yu, X. Zhou, J. Tang, D. Zhao, Highly ordered mesoporous bioactive glasses with superior in vitro bone-forming bioactivities, Angew. Chem. Int. Ed. 43 (2004) 5980–5984, https://doi.org/10.1002/anie.200460598.